



## EFFECT OF PARTIAL SUBSTITUTION OF CHROMIUM ON RARE EARTH STRONTIUM NANOSIZED HEXAFERRITES

S. A. Pawade<sup>1</sup>, V. M. Nanoti<sup>2</sup>, K. G. Rewatkar<sup>3</sup>

<sup>1</sup>Department of Applied Physics, Rajiv Gandhi College of Engineering,  
Chandrapur

<sup>2</sup>Department of Applied Physics, Priyadarshini College of Engineering,  
Nagpur

<sup>3</sup> Department of Physics, Dr. Ambedkar College, Nagpur

### Abstract

A stoichiometric Cr-substituted M-type Strontium Lanthanum Hexaferrites,  $\text{SrLaFe}_{12-x-y}\text{Cr}_x\text{O}_{19}$ , with  $x = 0$  to  $8$ , powder was synthesized by microwave assisted solgel auto-combustion route using urea as a reductant and nitrates as oxidants. The ferrites were systematically investigated by using powder X-ray diffractometer (XRD), magnetic hysteresis recorder, and Transmission Electron Microscope (TEM). (XRD) studies reveal that microwave-assisted combustion synthesis route yields materials with higher degree of compositional stability and phase purity. Both  $a$  and  $c$  lattice parameters calculated and found to decrease with increasing Cr content. The effects of  $\text{Cr}^{3+}$  ions on the Strontium Lanthanum ferrites were reported and discussed in detail. The site preference of  $\text{Cr}^{3+}$  and magnetic properties of the ferrites have been studied using hysteresis. The results show that the magnetic properties are closely related to the distributions of  $\text{Cr}^{3+}$  ions on the five crystallographic sites. The saturation magnetization slowly decreases, however, the coercivity decreases with Cr concentration. The magnetization results indicate that the  $\text{Cr}^{3+}$  ions preferentially occupy the  $2a$ ,  $12k$ , and  $4f_{VI}$  sites. TEM study reveals nanosized ferrites.

**Keywords:** Strontium ferrite, X-ray density, porosity, magnetization, coercivity, retentivity etc.



## 1. Introduction

Ferrite is a very important class of magnetic oxides which contains magnetic ions arranged in such a manner that it produces spontaneous magnetization while maintaining good dielectric properties. M-type Strontium hexaferrite ( $\text{SrFe}_{12}\text{O}_{19}$ ) are one of the hexagonal group having mechanical hardness, environmental chemical stability and excellent magnetic properties. The presence of large Strontium atoms causes the strontium hexaferrite to have high magnetic permeability unlike spinels and garnets.[1] The improved magnetic properties with proper substitutions make hexaferrite an active ingredient in magnetic recording media [2,3] Polycrystalline hexaferrites are also good dielectrics [4] and higher values of magnetic parameters makes them suitable for microwave applications[5].

Ever since the discovery of the Sr-M hexaferrites, extensive research has improved their magnetic capabilities. In order to improve the fundamental magnetic properties of hexaferrites, many studies have also been concerned with cationic substitutions. In general, many cations and various cationic combinations such as Al [6], Ga[6,7], Sc[7], In [7], Co-Ti [8], Co-Sn[9,10], Zn-Sn[11], Zn-Zr[12], Zn-Ti [13,14], etc., are doped into Sr-M ferrites. It is suggested that a combination of dopants can be used to control or reduce coercivities with only a small change of their saturation magnetizations [8-10]. Furthermore, the substitutions of Fe ions by isovalent cations can be generally investigated. The saturation magnetization and other properties are closely related to the distribution of the doping ions on five Fe crystallographic sites. In 1995 Wartewig [15] first investigated Cr distribution in Cr-doped Sr-M ferrites prepared by a solid state reaction. Mössbauer spectra of chromium-doped strontium ferrites found that the  $\text{Cr}^{3+}$  ions initially substituted Fe at 2a octahedral site and followed the preference on 12k and  $4f_{VI}$  octahedral sites, respectively, due to the crystal field effect. In

this report, the properties of Cr-substituted Sr-M ferrites,  $\text{SrLa}_y\text{Fe}_{12-x-y}\text{Cr}_x\text{O}_{19}$  ( $0 \leq x \leq 8$ ,  $y = 1$ ) are investigated and discussed [16].

The Sr-M hexaferrite structure is symbolically assigned as  $\text{RSR}^*\text{S}^*$  where R is a rhombohedral block forming a three-layer block (two  $\text{O}_4$  layers and one  $\text{SrO}_3$  layer) with composition as  $\text{Sr}^{2+}\text{Fe}_6^{3+}\text{O}_{11}^{2-}$  and S is a spinel block forming a two  $\text{O}_4$  layer block with composition as  $\text{Fe}_6^{3+}\text{O}_8^{2-}$ . The blocks signified by asterisk have been rotated by  $180^\circ$  about the c-axis. The Sr-M structure consists of five distinct Fe crystallographic sites, i.e., three octahedral (12k,  $4f_{\text{VI}}$  and 2a) sites, one tetrahedral ( $4f_{\text{IV}}$ ) and one trigonalbipyramid (2b) site [17].

Various chemical processes [18] have usually been adopted to prepare the Sr-M hexaferrites. Conventional solid-state reaction routes requires repeated grinding and calcinations steps to get the desired properties, which invariably contaminate the powders. Recently, combustion synthesis has emerged as an attractive technique for the production of homogeneous, high-purity, and crystalline oxide powders at significantly lower temperatures than the conventional synthesis methods requiring shorter time periods and using less amount of external energy as well [19-21]. Further, it has also been observed that the combustion-synthesized powders retain their nanocrystallite structure even after sintering, which is extremely useful in making super-plastic deformation materials.

## 2. Experimental details

Powders of  $\text{SrLa}_y\text{Fe}_{12-x}\text{Cr}_x\text{O}_{19}$  with ( $0 \leq x \leq 8$ ,  $y = 1$ ) were synthesized using a sol-gel auto combustion process. All chemicals used for this synthesis were of analytical reagent grade. The experimental sequence may be summarized as follows: A yellow-brown transparent aqueous solution of  $\text{Sr}(\text{NO}_3)_2$ ,  $\text{Fe}(\text{NO}_3)_3 \cdot 9\text{H}_2\text{O}$ ,  $\text{Cr}(\text{NO}_3)_3 \cdot 9\text{H}_2\text{O}$ ,  $\text{La}(\text{NO}_3)_3 \cdot 6\text{H}_2\text{O}$ ,  $\text{CO}(\text{NH}_2)_2$  was prepared. The solution was heated under constant stirring at a temperature of about  $140^\circ\text{C}$  in a Pyrex beaker so that it

concentrated slowly without producing any precipitation, but changed its viscosity and color, until it turned into a brown gel. When the temperature of the microwave oven was raised to about 250–300 °C, the gel swelled into foam and underwent a self-propagating combustion reaction changing the brown gel into black powders. The entire combustion process was over after half an hour. The resulting black ashes were ground in an agate mortar, put into alumina crucibles, and then calcined at 1100°C for 1h until complete decomposition of the carbonaceous residues and solid state reaction occurred. The calcined powders were ground and sieved through 200 meshes. These powders and 10% polyvinyl acetate (PVA) solution (2–3 drops) had been mixed before they were pressed into pellets of 15 mm in diameter and about 2–4mm in thickness using a stainless steel die set under uniaxial pressure of 15 tonnes/inch for 10 min. This gave several pellets of each composition which were then sintered at 1200 °C in flowing oxygen atmosphere for 12h. During sintering process, the crystallization gave rise to a hexagonal polycrystalline phase. Fig.1 shows modified version of domestic microwave oven used in the present work having 2.45 GHz frequency.



**Figure 1.** Modified domestic microwave oven used for synthesis of  $\text{SrLa}_y\text{Fe}_{12-x-y}\text{Cr}_x\text{O}_{19}$ .



### 3. Results and discussion

Hexaferrite  $\text{SrFe}_{12}\text{O}_{19}$  was first prepared by AdelsKold in 1983(22). He also determined the crystal structure of this compound to be iso-structural with magnetoplumbite(M) With space group  $P6_3/mmc$ . The lattice parameters measured are  $a = 5.8863\text{\AA}$  and  $c = 23.0376\text{\AA}$  at room temperature [23]. In the present investigation  $\text{Cr}^{+3}$  substituted  $\text{SrFe}_{12}\text{O}_{19}$  ferrites were synthesized by sol-gel auto combustion technique. Fig 2 shows XRD pattern of high purity Cr doped strontium ferrites with different doping concentrations. All peaks belongs to M-structure ferrite phase and no intermediate phases are observed. The lattice parameter 'a' and 'c' are in the range of 5.5-6 Å and 23.15 to 23.55 Å pertaining to SG:  $P6_3/mmc$  (no. 194). It is also seen that 'a' and 'c' decrease slightly to increase in  $\text{Cr}^{+3}$  concentration. The substitution does not affect much on the crystal symmetry (table- 2). This due to relatively small ionic radii of  $\text{Cr}^{+3}$  (0.64Å) (comparing with that of Fe (0.67Å) for six fold coordination. As a result the cell volume of the compounds decreases after being doped.

There are two formula units in a unit cell. There are ten layers of Oxygen atoms along the c-axis. The structure built up from small units: a cubic block (S) having the spinel

Table 1. Crystallographic sites of Fe ions.

| Sub lattice     | Co-ordination          | Number of ions | Spins |
|-----------------|------------------------|----------------|-------|
| 12K             | Octahedral             | 6              | Up    |
| 4f <sub>1</sub> | Tetrahedral            | 2              | Down  |
| 4f <sub>2</sub> | Octahedral             | 2              | Down  |
| 2a              | Octahedral             | 1              | Up    |
| 2b              | Trigonal bi- pyramidal | 1              | Up    |

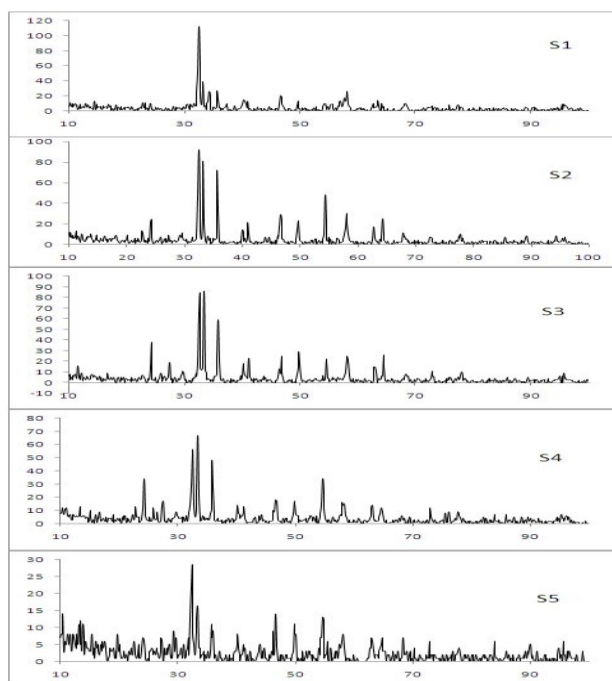


**Figure 2.** XRD pattern at room temperature of  $\text{SrLa}_y\text{Fe}_{12-x-y}\text{Cr}_x\text{O}_{19}$ .

type structure and a hexagonal (R) block containing  $\text{Sr}^{+2}$  ions. The iron atoms are positioned at five crystallographically different sites as shown in table-1.

Fig. 3 shows the hysteresis loops of  $\text{SrLa}_y\text{Fe}_{12-x-y}\text{Cr}_x\text{O}_{19}$  with ( $0 \leq x \leq 8$ ,  $y = 1$ ) under high magnetic field (15 KOe). Absolutely there is no constriction in  $\text{SrLaFe}_{11}\text{O}_{19}$ . Absence of constriction in

**Table2.** Lattice Parameters, X-Ray Density, Particle Size and Porosity  $\text{SrLa}_y\text{Fe}_{12-x-y}\text{Cr}_x\text{O}_{19}$

| Samples | x | Molecular Weight (gm/mol) | 2θ    | Lattice Parameters |        | c/a (Å) | X Ray Density (gm/cm <sup>3</sup> ) | Bulk Density (gm/cm <sup>3</sup> ) | Porosity (%) | Particle Size (Å) | Volume (Å <sup>3</sup> ) |
|---------|---|---------------------------|-------|--------------------|--------|---------|-------------------------------------|------------------------------------|--------------|-------------------|--------------------------|
|         |   |                           |       | a (Å)              | c (Å)  |         |                                     |                                    |              |                   |                          |
| S 1     | 0 | 1144.8091                 | 32.42 | 5.826              | 23.527 | 4.038   | 5.496                               | 2.777                              | 49.4         | 7.237             | 691.65                   |
| S 2     | 2 | 1137.1111                 | 32.47 | 5.819              | 23.481 | 4.035   | 5.462                               | 2.619                              | 52.7         | 36.19             | 691.27                   |
| S 3     | 4 | 1145.4137                 | 32.52 | 5.812              | 23.435 | 4.030   | 5.549                               | 2.428                              | 54.5         | 12.065            | 688.68                   |
| S 4     | 6 | 1145.7157                 | 10.95 | 5.805              | 23.356 | 4.035   | 5.546                               | 2.399                              | 56.3         | 34.908            | 685.98                   |
| S 5     | 8 | 1146.0179                 | 32.37 | 5.794              | 22.206 | 3.832   | 5.894                               | 2.377                              | 59.4         | 7.617             | 645.66                   |

**Table 3** Electrical Conductivity Calculations for the samples  
 $\text{SrLaCr}_x\text{Fe}_{11-x}\text{O}_{19}$

| Samples | x | Resistivity<br>( $\rho$ ) at 300<br>K<br>( $\Omega\text{-cm}$ ) | Capacitance<br>(F) | Dielectric<br>Loss<br>Factor( $\epsilon$ ) | $\Delta E$ (eV) |         | Transition<br>Temperature<br>$T_d$ (K) | Curie<br>Temperature<br>$T_c$ (K) |
|---------|---|---|--------------------|--|-----------------|---------|--|-----------------------------------|
|         |   |   |                    |  | Para            | Ferri   |  |                                   |
| S 1     | 0 | 1.23E+07  | 3.19E-11           | 4.28E-10                                   | 0.30261         | 0.6222  | 473                                    | 475                               |
| S 2     | 2 | 3.31E+05  | 2.46E-10           | 1.25E-08                                   | 0.58824         | 0.44837 | 513                                    | 518                               |
| S 3     | 4 | 1.22E+04  | 7.85E-09           | 1.02E-03                                   | 0.65882         | 0.34542 | 523                                    | 528                               |
| S 4     | 6 | 2.27E+05  | 1.26E-10           | 1.47E-10                                   | 0.732           | 0.31895 | 583                                    | 590                               |
| S 5     | 8 | 2.11E+07  | 3.19E-11           | 4.28E-10                                   | 1.07941         | 0.2641  | 598                                    | 604                               |

**Table 4** VSM Calculations for  $\text{SrLaCr}_x\text{Fe}_{11-x}\text{O}_{19}$

| Samples | x | Saturation<br>Magnetization<br>(emu/g) | RetentivityMr<br>(emu/g) | Coercivity<br>(Oe) | Bohr<br>Magneton<br>( $\mu_B$ ) | Anisotropy<br>Constant<br>(K) | Mr/Ms |
|---------|---|--|--------------------------|--------------------|---------------------------------|-------------------------------|-------|
| S 1     | 0 | 861.6                                  | 453.8                    | 5375               | 176.616                         | 2.32E+00                      | 1.899 |
| S 2     | 2 | 59.11                                  | 77.54                    | 2250               | 14.16                           | 2.38E-03                      | 1.955 |
| S 3     | 4 | 18.85                                  | 21.04                    | 1250               | 0.42                            | 3.23E-02                      | 2.459 |
| S 4     | 6 | 0.372                                  | 0.071                    | 1000               | 0.39                            | 1.86E-04                      | 5.209 |
| S 5     | 8 | 0.334                                  | 0.032                    | 125                | 0.069                           | 2.09E-05                      | 10.61 |

$\text{SrLaFe}_{11}\text{O}_{19}$  may imply existence of a certain contact between constricted loops and the ionic contents of both Cr and Fe elements. While the reason for no constriction in  $\text{CrLaFe}_{11}\text{O}_{19}$  could not be explained using Jida's results since there is no clue of the influences of cation ratio on directional ordering in this theory [24]. We therefore assumed that the exchange interaction between  $\text{Cr}^{+3}$  and  $\text{Fe}^{+3}$  and ions within a certain distance on the interstitial side may play a crucial role in this phenomenon. In addition we have investigated the effect of aging time on the constriction of hysteresis (Not shown here), and found that there is hardly any difference between samples 10 hrs to 50 hrs. Considering the migration of ions on tetrahedral / Octahedral sites which happens very



quickly, it seems that the mechanism of this constriction is quite local and forms in a relatively short period of time. Another reason for constriction free loop, which may attribute to larger crystal lattice compared to the aged sample which will influence the interaction between cations/anions and hence repressed the constriction.

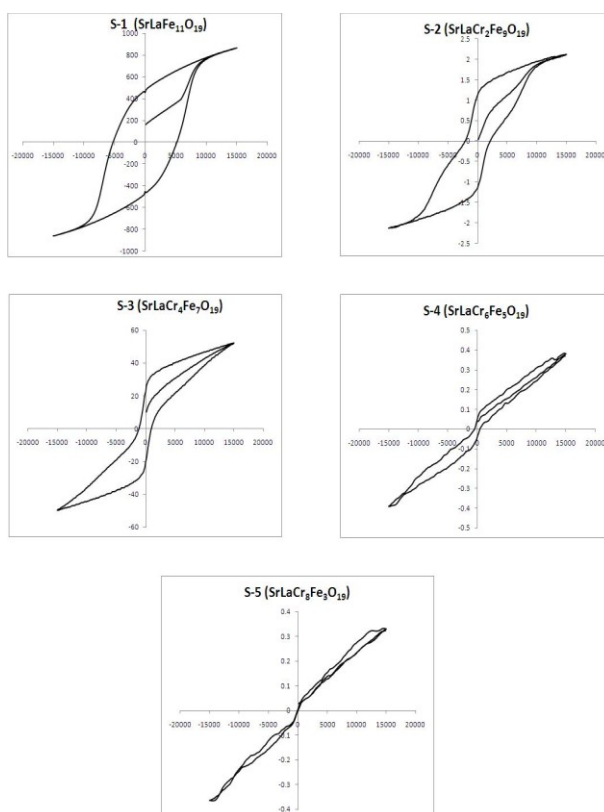


**Figure 3.** Room temperature hysteresis of  $\text{SrLa}_y\text{Fe}_{12-x}\text{Cr}_x\text{O}_{19}$

Partial substitution of  $\text{Fe}^{3+}$  by  $\text{La}^{3+}$  in the reported ferrites has shown an increase in the coercive field about 2kOe ( $\approx 30\%$  increase) than a pure substituted due to the contribution from the large single ion anisotropy from rare earth sublattice. Similar results are reported by [25] in case of partial substitution of  $\text{Fe}^{3+}$  by  $\text{Tb}^{3+}$  and  $\text{Dy}^{3+}$  ions in cobalt ferrite system. Substitution of rare earth ion into the spinel structure has been reported to lead to structural distortion [26] and to induce strains in the materials and significantly modify the magnetic and electric behavior.

The particle morphology was examined by Transmission Electron Microscope (TEM). The particle size was in nano scale ( $\approx 52$  nm) (Fig. 4).



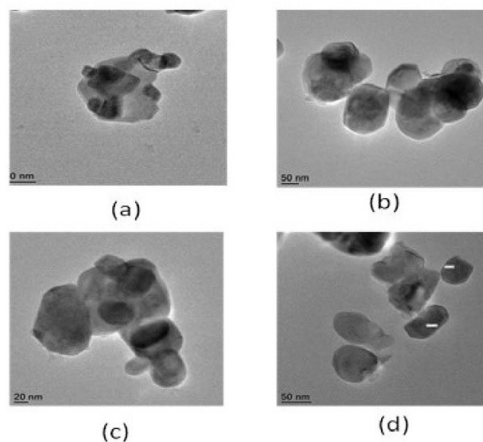


**Figure 4.** TEM of  $\text{SrLa}_y\text{Fe}_{12-x-y}\text{Cr}_x\text{O}_{19}$ , where (a) S1, (b) S2, (c) S4, (d) S5. The effect of  $\text{Cr}^{+3}$  ions on the saturation magnetization, retentivity and coercivity of compounds under study are shown in Fig. 5. The increase of  $\text{Cr}^{+3}$  ions content, the saturation magnetizations deduced from law of approach to saturation show the decrease in coercivities.

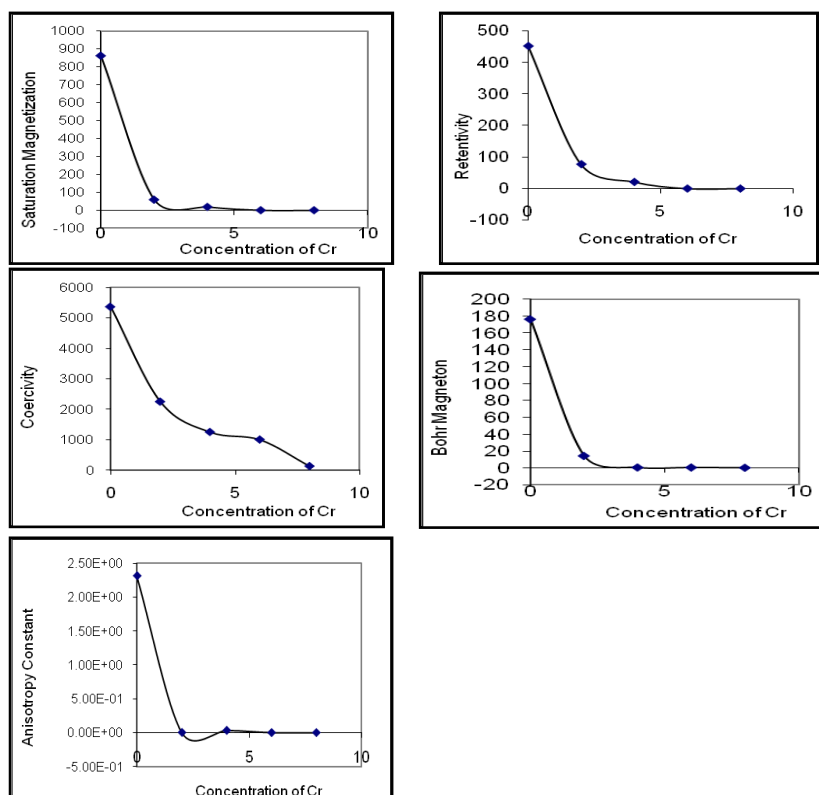


**Figure 5.** Variation of magnetic parameters for the compounds  $\text{SrLa}_y\text{Fe}_{12-x-y}\text{Cr}_x\text{O}_{19}$ .



The magnetizations are closely related to distribution of  $\text{Cr}^{+3}$  ions on each crystallographic sites and then magnetic dilution or non-collinear structure (spin canting) with the substitution of  $\text{Fe}^{+3}$  ions by lower magnetic movement ions, in this case  $\text{Cr}^{+3}$  ions.

It is evident that the areas on octahedral 12k and  $4f_{VI}$  sites tend to decrease with the doping content. In other words this means that the  $\text{Cr}^{+3}$  ions could be entering into the octahedral 12k and  $4f_{VI}$  sites. From magnetic results, it should be noted that  $\text{Cr}^{3+}$  ions preferentially occupy on octahedral 12k, 2a and  $4f_{VI}$  sites resulting in the dramatic drop in saturation magnetization and the lowering of the Curie temperature. The  $\text{Fe}^{3+}\text{-O-Fe}^{3+}$  super exchange interaction would be partially disrupted by substituting  $\text{Fe}^{3+}$  with  $\text{Cr}^{3+}$  on 12k site. Furthermore, it is known that for each  $4f_{IV}$  site, there are three neighboring 12k sites and the preference of  $\text{Cr}^{3+}$  ions on 12k site strongly perturbs the 12k- $4f_{IV}$  magnetic super exchange interaction.

The site occupancies as determined by Mössbauer spectra show that the lanthanum cations prefer to occupy the  $4f_{IV}$ , 12k, and 2b sites [27]. Site occupancy of  $4f_{IV}$ , 12k, and 2b sites have an effect on variation of magnetic properties, as seen in the present case.

The structure with octahedral Fe at  $4f_{VI}$  having antiparallel spin has a lower energy than that tetrahedral Fe at  $4f_{IV}$  sites. The structure with antiparallel spin at 12K has a very low energy compared with the ferromagnetic structure. Furthermore, the calculations showed that the among the five different  $\text{Fe}^{+3}$  ions at Fe (2a) site there is the small number of electrons (2.65 electrons). While there is the largest number of electron at the Fe ( $4f_{IV}$ ) site (3.09 electrons) which is in agreement with bondvalancies.

The  $\text{Cr}^{+3}$  substituted compounds of  $\text{CrLaFe}_{11}\text{O}_{19}$  showed pronounced constriction. This phenomenon may be attributed to the distortion of



lattice and subsequently the variety of uniaxial anisotropy, which is due to changes of inner and/or inter ratios between ions and vacancies. The magnetic structure of  $\text{CrFe}_{12}\text{O}_{19}$  is ferromagnetic; there is no pinning effect between the interstitial sites. The constriction may be regarded as disproof of the shape effect [25, 26] originated anisotropy of Sr-ferrites. Further investigations like crystal and domain structure under low temperature should be taken in consideration and a new mechanism rather than thermal fluctuations and thickness-variety of Bloch Wall for high and low temperature [27] needs to be established.

In case of samples  $\text{SrLaCr}_6\text{Fe}_5\text{O}_{19}$  and  $\text{SrLaCr}_3\text{Fe}_3\text{O}_{19}$  the noisy regions in hysteresis are observed. The starting magnetization for these compounds exhibit comparably large amplitude oscillations at the vibrating frequency  $f/2$ , the phases of which are very different. However, after attainment of saturation these larger amplitude vibrations gets suppressed to large extend and are replaced by small amplitude vibrations at frequency ' $f$ '. We note that in the first oscillation are present on both side of the central, post and pre saturation hysteresis loop, show additional small amplitude, higher frequency oscillations, which may be higher harmonics of ' $f$ '. This occurrence may be due to randomness of the oscillation phases, lead to starting magnetization curves that are very different from those that start at the saturation magnetization, but are subsequently identical. That is after the attainment of saturation the configurations are identical. The figure demonstrates that steps in the magnetization do not necessarily have unusual hysteresis effect.

#### **4. Conclusions**

All the synthesized compounds shows magnetoplumbite (M) structure with single phase. The grain size of the samples is in the range of nano size ( $\approx 52$  nm). The partial substitution of rare earth  $\text{La}^{+3}$  ions for  $\text{Fe}^{+3}$  had enhanced the total coercive field by almost 30%. The saturation



magnetizations are closely related to the distribution and concentration of  $\text{Cr}^{3+}$  ions on the five crystallographic sites. Magnetic results revealed that  $\text{Cr}^{3+}$  ions preferentially occupy the octahedral 2a, 4f<sub>2</sub>, and 12k sites. With  $\text{Cr}^{3+}$  entering the  $\text{Fe}^{3+}$  crystallographic sites, the saturation magnetization dramatically falls and coercivity also shows decreasing trend. The decrease in magnetization is therefore attributed to  $\text{Cr}^{3+}$  ions occupying on the spin up Fe sites (2a and 12k sites) and magnetic dilution or non-collinear structure. It is evident that the  $\text{Fe}^{3+}\text{-O-Fe}^{3+}$  super exchange interaction may be weakened by  $\text{Cr}^{3+}$  ( $3d^3$ ) substituting into some  $\text{Fe}(3d^5)$  sites.

### References :

- Kulkarni D C, Patil S P, and Puri Vijaya (1995) *J. Magn. Magn. Mater.* 2089 140
- Haneda K, and Morrish A H, (1990) *Phase Transitions* 24 661
- Wang X, Lu D Li, L, and Wang X, (1996). *J Alloys Comp* .273 661
- Ismeal H, Nimr M K El, Ata A M Abouel, Elhiti M A, Ahmed M A, and Murakhowski A A (1995). *J. Magn. magn. Mater.* 150 403
- Kulkarni D K, Sawadh P (2000) *Mater. Chem. Phys.* 63 (2), 170.
- Currie R A Mc, (1994) *Ferromagnetic Materials: Structure and Properties*, Academic Press Limited, London, 180–181 & 234–246.
- Clark T M, Evans B J, and Thomson G K, (1999 ). *J. Appl. Phys.* 85 5229.
- An S Y, Shim I B, and Kim C S, (2002). *J. Appl. Phys.* 91 (10) 8465.
- Zhou X Z, Morrish A H, Yang Z, and Zeng, (1994). *J. Appl. Phys.* 75 (10) 5556.
- Han D H, Yang Z, Zeng H X, Zhou X Z, and Morrish A H, (1994). *J. Magn. Magn. Mater.* 137, 191.
- Fang H C, Yang Z, Ong CK, Y Li, and Wang C S, (1998). *J. Magn. Magn. Mater.* 187 129.
- Li Z W, Ong C K, Yang Z, Wei FL, Zhou X Z, and Zhao (2000 ). J.H., *Phys. Rev. B* 62 (10) 6530.



- Wang C S, Wei F L, Lu M, Han D H, and Yang Z, (1998 ). *J.Magn. Magn. Mater.* 183 241.
- Wartewig P, Krause M K, Esguinazi P, Rosler S, and Sonntag R, (1999 )  
*J. Magn. Magn. Mater.* 192 83.
- Wartewig P, Melzer K, Krause M, and Tellgren R, (1995). *J. Magn. Magn.Mater.*140–144 2101.
- Ounnunkad S, and Winotai P (2006). *Journal of Magnetism and Magnetic Materials* 301, 292-300,
- Kojima H, in: Wohlfarth E.P. (Ed.), (1982)*Ferromagnetic Materials: A Handbook on the Properties of Magnetically Ordered Substances*, North-Holland, Amsterdam, , p. 305
- Ganesh I, Bhattacharjee S, Saha B P, Johnson R, and Mahajan Y R (2001). *A new sintering aid for magnesium aluminate spinel*, *Ceram. Int.* 27, 773–779
- Mimani T, *Instant synthesis of nanoscale spinel aluminates* (2001). *J. Alloys Compd.*315 123–128.
- Ganesh I, Srinivas B, Johnson R, Saha B P, and Mahajan Y R, (2002).  
*Br. Ceram. Trans.*101 (6) 247–256.
- Ganesh I , Srinivas B , Johnson R , Rao G V N , and Mahajan Y R , (2003 ). *J. Ceram. Trans.* 102 (3) 119–128.
- Adelskold V , and Arkiv Kami Min Geol, (1983). A 12, 1-9
- Obradors X, Solans, Kimura X, Collomb A, Samaras D, and Rodriguez J, (1988). PernetMemd Font-Altaba M, *J. Solid State Chem.*72, 218.
- Iida S, Sekizawa H, and Aiyama Y, (1955). *J. Phy. Soc. Jpn.* 10 907
- Cheng F, Liao C, Kuang J, Xu Z, Yan C, Chen L, Zhao H, and Liu Z (1999)  
*J. Appl. Phy.*85 2782
- Rezlescu N, and Rezlescu E (1994). *J. Phys: Condens Matter*6 5707
- Dong H C, Lee W, Shim In-Bo, and Kim C S (2006 ). *J. Magn. Magn. Mater.* 304 243